Nanoscale

PAPER

View Article Online
View Journal | View Issue

Cite this: *Nanoscale*, 2025, **17**, 7844

Nanoparticles alter locust development and behaviour†

Preetam Kumar Sharma, ‡[a,b] Liya Wei, ‡[c] Atul Thakur,[d,g] Jialing Pan,[c] Chang Chen,[c] Navneet Soin,[a,e,f] Le Kang *[c] and Nikhil Bhalla *[a]

Received 27th November 2024,
Accepted 17th February 2025

DOI: 10.1039/d4nr04993d

rsc.li/nanoscale

Locusts, among the world's most destructive migratory pests, threaten food security by devastating crops and pastures. Conventional chemical insecticides pose environmental and health risks, highlighting the need for sustainable alternatives. We demonstrate the efficacy of nickel ferrite ($NiFe_2O_4$) nanoparticles (36 ± 10 nm), as a safe, cost-effective insecticide for locust management. These $NiFe_2O_4$ nanoparticles disrupt locust development by impairing blastokinesis and growth, thus resulting in malformed nymphs with compacted abdomens and disorganised body structures – primarily arising from significantly lower heart rates (30 bpm for control *vs.* 20 bpm for embryos exposed to $NiFe_2O_4$) and changes to end-diastolic and end-systolic dimensions. Adult locusts retained ingested nanoparticles in their coelomic cavities, which could potentially be used as traceable markers for swarm tracking. Additionally, the nanoparticles were recoverable from soil with over 90% efficiency, minimising potential ecological impact. Our research therefore offers an innovative nanotechnology-based solution for sustainable and effective locust management.

Introduction

Locust species inhabit all continents except Antarctica.[1] Among these, the desert locust (*Schistocerca gregaria*) and the migratory locust (*Locusta migratoria*) present significant challenges owing to their wide geographical distribution and extraordinary migratory capabilities.[2–4] Both these species exhibit the unique ability to multiply rapidly and transition from solitary to gregarious behaviour in response to population density increases, forming massive swarms.[5,6] These swarms, which are among the world's most destructive groups of migratory pests, cause crop damage so extensive that they threaten the food security of millions of people in underdeveloped and developing nations. Historical records of *Locusta migratoria* date back to as early as 707 BC in ancient Chinese documents, highlighting the enduring challenge of locust management.[7,8] More recently, the Food and Agriculture Organisation of the United Nations (FAO-UN) has warned that, without immediate interventions, locust outbreaks could escalate into catastrophic plagues within the next decade.[9–12] Consequently, addressing the threat posed by these voracious creatures in agricultural fields has become a global challenge that demands urgent attention.[2]

The crisis has been further exacerbated by the unpredictable weather patterns driven by climate change, which are expected to further intensify locust activity.[13–16] Traditional chemical control pathways reliant on pyrethroid-based and organophosphate-based insecticides have several shortcomings including high organic solvent content, poor dispersibility in soil and poor specificity against the target pests.[15,17] Furthermore, the low target efficiency of pesticides results in a staggering 90% of the formulation running off into the environment.[13] Consequently, these factors contribute to severe environmental pollution, posing significant risks to human health, aquatic life, domestic animals, birds, insect populations, and soil microbes, while also burdening farmers with higher operational costs.[16] Shifting climate conditions and the rapid emergence of insecticide resistance therefore demand nanotechnology-based approaches to solve these grand challenges *via* precision agricultural technologies.[18] As such, several nanomaterial types, including polymers, lipids, ceramics, and metals, have been leveraged for pesticide formu-

[a]*Nanotechnology and Integrated Bioengineering Centre (NIBEC), School of Engineering, Ulster University, York Street, Belfast, Northern Ireland, BT15 1AP, United Kingdom. E-mail: n.bhalla@ulster.ac.uk*
[b]*Institute for Materials Discovery, University College London, Malet Place, London, WC1E 7JE, United Kingdom*
[c]*Institute of Life Science and Green Development/Hebei Basic Science Center for Biotic Interaction, College of Life Science, Hebei University, Baoding 071002, China. E-mail: lkang@ioz.ac.cn*
[d]*School of Electronics and Information Engineering, Nanjing University of Information Science & Technology, 210044 Nanjing, China*
[e]*School of Science, Computing and Engineering Technologies, Swinburne University of Technology, Hawthorn, Victoria 3122, Australia*
[f]*School of Science, RMIT University, Melbourne, Victoria 3001, Australia*
[g]*Amity Institute of Nanotechnology, Amity University Haryana, Gurugram, 122413, India*

†Electronic supplementary information (ESI) available: Additional information and figures. See DOI: https://doi.org/10.1039/d4nr04993d

‡These are joint first authors of this work.

lations. These are collectively categorised as nanopesticides, and used against insects, mites, and microorganisms.[19] Nanopesticides provide several beneficial characteristics that set them apart from conventional chemical pesticides. They offer a larger surface area, and superior dispersion in various solvents including water, simple attachment, controlled release, rapid mass transfer, and diminished residuals in the environment.[14,20–24] Analysis by Wang *et al.* has shown that nanopesticides have a 31.5% higher efficacy towards the target organism (as compared to bulk counterparts) with a 22.1% lower leaching potential, while being able to mitigate biotic and abiotic stresses (heat, drought, salinity *etc.*).[22]

In previous studies, we have demonstrated the efficacy of cobalt and nickel ferrites as microbial pesticides against plant pathogenic fungi.[25] Fungi, being eukaryotic microorganisms, differ fundamentally from Acrididae (locusts), which are highly complex multicellular organisms. Based on these differences, it can be assumed *a priori* that the effectiveness of ferrites against fungi would not mean they are effective against locusts. However, recent findings challenge this assumption. For instance, studies on zinc chromium oxide nanoparticles have shown their efficacy against *Schistocerca gregaria.*[26] The ZnCrO nanoparticles were shown to cause structural damage to fat body cells in immature locust stages, disrupt cellular functions, and, at higher concentrations, lead to nymphal death by altering development.[26] It should be noted that magnetic nanoparticles, owing to their size, composition, aggregation and surface charge, show varying levels of cellular uptake and bioactivity towards cells and tissues.[27,28] For instance, while magnetic iron oxide nanoparticles have been shown to have limited toxicity (at low loadings),[29,30] nickel ferrite nanoparticles are known to generate reactive oxygen species (ROS)[31] upon interaction with biological tissues leading to oxidative stress, and cause disruption of processes like cell division, protein synthesis, and morphogenesis. Nickel ferrite nanoparticles have also been linked to severe myocarditis, neuron necrosis, and other pathological conditions.[32] Similarly, cobalt ferrite nanoparticles have been associated with developmental malformations, including cardiac edema, delayed hatching and apoptosis with oxidative stress being a key contributor.[33] Despite these studies, the potential insecticidal activity of ferrites, including their mechanisms of action against Acrididae species, remains largely unexplored. Further investigation into this area could reveal novel dual-function compounds for pest and fungal control.[34]

In this work, we have sought to develop a mechanistic understanding of the use of magnetic nickel ferrite ($NiFe_2O_4$) nanoparticles, in addressing the locust crisis. Our comprehensive investigation covers several aspects including the design and physicochemical characterisation of nanoparticles, simulating the natural habitat of locusts under laboratory conditions for growing them, exhibiting mechanisms which show how the nanoparticles reach the eggs buried in soil, and crucially, examining the nanoparticle–locust interaction at both embryonic and adult stages. Our findings reveal that $NiFe_2O_4$ nanoparticles effectively curtail the transition of eggs into healthy nymphs by causing delays in embryonic development and blastokinesis processes. Additionally, it was observed that the heart rate of the embryos decreased, which resulted in abnormal physical characteristics in the nymphs. Lastly, we demonstrate a method to recover unutilised nanoparticles from the soil, ensuring both cost efficiency and minimal environmental impact.

Nikhil Bhalla

Nikhil Bhalla is currently working as a lecturer (assistant professor), at the University of Ulster, UK. His research interest is in biosensing with a prime focus on nanoplasmonic technologies and interfacial science of biosensing materials, transducers, and biorecognition layers. He focuses on the use of his developed sensors for healthcare and food applications. He did his postdoctoral training at OIST, Japan with Professor Amy Shen after receiving his Ph.D. from the University of Bath, UK, in 2016, M.S. in microelectronics and applications from CYCU, Taiwan and a first division honours degree (B.E. Hons) in electronics and instrumentation engineering from BITS-Pilani, India.

Results and discussion

Nanoparticle characterisation

Nickel ferrite ($NiFe_2O_4$) magneto-plasmonic nanoparticles, referred to as MNPs hereafter, were synthesised using the co-precipitation method.[25,35] A brief description of the process can be found in the ESI.† The MNPs were primarily assessed for their size, shape and crystalline structure. Transmission electron microscopy (TEM) revealed an average size of 36 ± 10 nm, as shown with the corresponding morphology in Fig. 1a (top-left). The crystalline nature of the nanoparticles was further studied using X-ray diffraction (XRD), selected area electron diffraction (SAED) and Raman spectroscopy. Analysis of the XRD pattern revealed diffraction peaks corresponding to the 111, 220, 311, 400, 440, and 511 planes of nickel ferrite (JCPDS Card no. 10-0325), as shown in Fig. S1a.†[25,36] The Raman spectrum (Fig. S1b†) exhibited active modes at 211 cm^{-1}, 331 cm^{-1}, 479 cm^{-1} and 696 cm^{-1}, consistent with the predicted positions.[37] Further analysis using scanning electron microscopy and energy dispersive X-ray (EDX) analysis (Fig. S1c†), revealed polyhedral ferrite nanoparticles and prominent peaks corresponding to O, Fe and Ni, confirming the nickel ferrite structure. The SAED pattern shown in Fig. 1 (inset, top-left) and interplanar spacings from high-resolution TEM, shown in Fig. S1d,† corroborate the findings from the XRD analysis.[38]

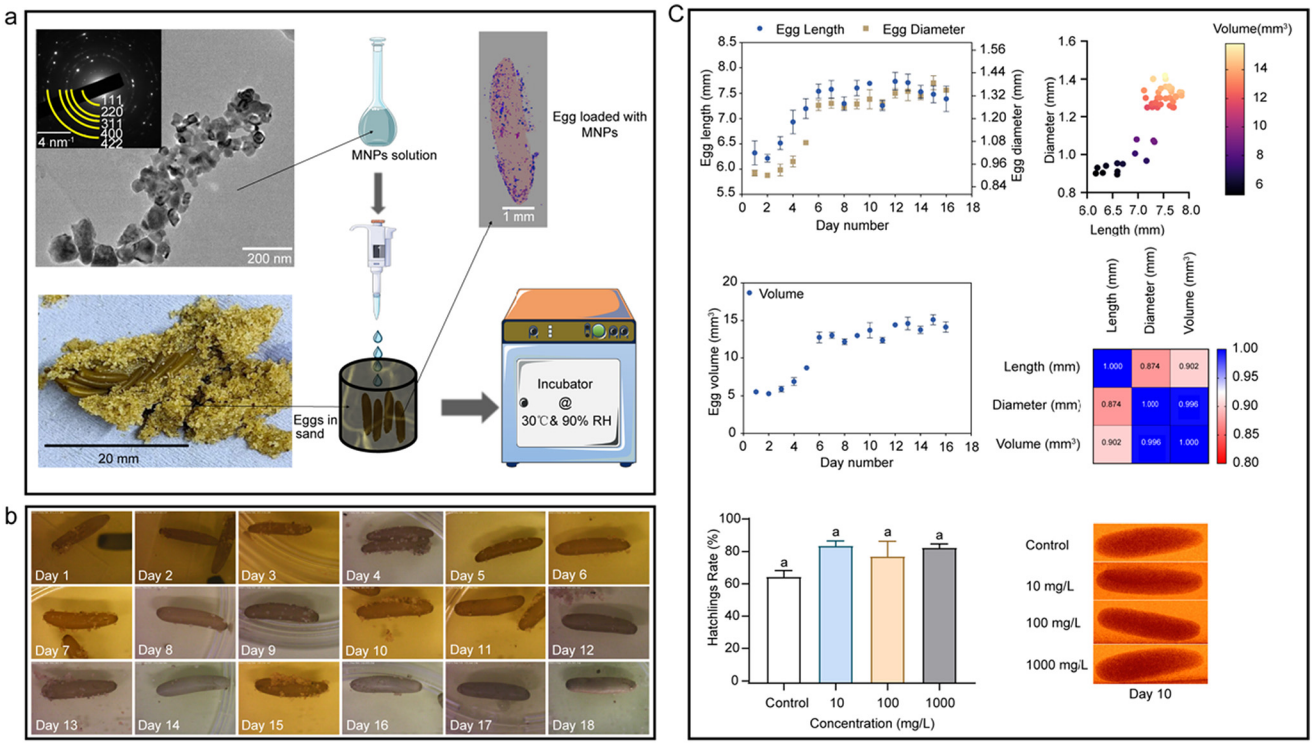

Fig. 1 Physical characterisation of MNPs and their effect on locust egg development. (a) TEM image and SAED pattern (inset) of Ni ferrite nanoparticles (top left). Image of an egg pod surrounded by sand and its changes (bottom left). Additionally, the arrows indicate the procedure for application of MNPs to the locust eggs where MNPs are added to the jar containing eggs buried in sand. These are kept in an incubator, which is maintained at 30 °C with a controlled relative humidity (RH) of 90%. An X-ray microtomogram (μCT) of individual eggs exposed to MNPs is also shown indicating that MNPs successfully reach the eggs. (b) Digital images of eggs during the growth period and (c) the change in length, diameter and volume of the eggs of migratory locusts over time. Hatching rate (bottom-left) and μCT (bottom-right) of eggs in the presence of various MNP concentrations. Statistical analysis was performed using multiple comparisons in a one-way ANOVA test. The same letter "a" indicates no significant difference while different letters indicate significant differences ($P < 0.05$). Bars represent the mean ± SEM (standard error of the mean). Each group has three biological replicates, with 100–130 eggs in one replicate.

Effect of MNPs on locust egg development

We first examine the impact of MNPs on egg development as part of a strategy to mitigate the effects of locust infestations, particularly during the egg development phase. Egg pods from the desert-type and migratory-type locusts were received in a jar (image in Fig. S2†). A representative image of the egg pod outside the jar is shown in Fig. 1a (bottom-left). In the schematic of Fig. 1a, we illustrate the process of exposing the locust eggs to MNPs (dispensed using a pipette and then incubated). Micro-computed tomography (μCT) imaging confirmed the interaction between the MNPs and the eggs. Embryonic development was carefully monitored for 18 days, as depicted in Fig. 1b.[39,40] Over this period, we observed a 22% increase in the length and a 55% enhancement in the diameter of the ready-to-hatch eggs compared to freshly laid eggs (Fig. 1c). Notably, after day 8, and through days 15–16, no significant changes were observed in the diameter, length, or volume of the eggs, as shown in Fig. 1c.

During the growth period, the egg volume increased threefold, consistent with earlier investigations on egg development in locusts.[41,42] To determine the effect of MNPs on the eggs, three different concentrations of MNPs, 10 mg L^{-1}, 100 mg L^{-1} and 1000 mg L^{-1} referred to as low, medium and high concentrations/loadings henceforth, were tested alongside a control group. The details are given in the Materials and methods section.

Nymphs began to emerge after 14 days, with all nymphs emerging within 18 days.[43] After 20 days, assuming no further eggs would hatch, the number of nymphs was counted. For low MNP loading, 82–90% of nymphs emerged as compared to 60–88% for medium loadings and 80–88% for high MNP loadings, as shown in Fig. 1c (bottom-left). Statistical analysis revealed no significant difference in hatchability between the three MNP loading treatments, suggesting that MNP concentration does not significantly affect the rate of egg development into nymphs. This observation is attributed to the fact that the eggs are randomly dispersed in the soil, meaning that the number of particles reaching the eggs after surface spraying of the topsoil is independent of the location of the eggs. This finding aligns with our μCT studies on nanoparticle movement in soil (discussed in the following sections), highlighting the challenge of controlling the number of nanoparticles that reaches the eggs at varying nanoparticle concen-

trations in the water solution. In contrast, the control group had a lower hatchability rate (60–73%), see Fig. 1c, and this disparity was found to be statistically significant as compared to the hatchability observed in the MNP-exposed experiments. To ensure that no additional nymphs were likely to emerge, a separate series of experiments – both in the presence and absence of MNPs – considered the development of eggs for a total of 35 days. After 20 days, no further nymphs emerged, providing confidence in the accuracy of the data.

Analytical techniques were utilised to investigate the translocation of MNPs within the locusts. As shown in Fig. 1a (top-right), MNPs can be seen inside the egg (as patches) in the case of low MNP loading. Additional images indicative of MNPs as patches on the surface of the eggs are presented in Fig. S3.† The overlapping EDX maps of Fe, Ni and O, confirm the presence of MNPs on the surface of the locust egg, providing further evidence of their interaction and the potential impact on the development of the eggs. It should be noted that smaller MNPs were more effectively internalized, potentially through surface pores or microchannels.[44] These physical interactions likely create a localized barrier, restricting nutrient exchange or gas diffusion – critical for embryonic development. As shown in the following sections, the μCT imaging reveals the accumulation of MNPs within embryonic tissues, suggesting their ability to cross the eggshell barrier.[44] This targeted deposition amplifies localized effects, such as oxidative stress and mechanical disruption, in key developmental sites. In this context, the presence of MNPs within embryonic tissues triggers the generation of reactive oxygen species (ROS), either directly through their chemical reactivity or indirectly *via* disruption of mitochondrial activity. Elevated ROS levels induce oxidative stress, which damages cellular components such as proteins, lipids, and DNA.[27,45–47] This contributes to developmental delays, structural deformities, and reduced hatchability observed in treated eggs (as discussed in the next section).

MNP-induced blastokinesis delay and abnormal cardiac activity

Fig. 2a shows that locusts exposed to MNPs during embryonic development and the blastokinesis process exhibited a slight developmental delay compared to the control group. This delay led to the emergence of abnormal nymphs, characterised by deformities such as severe abdominal compaction and disorganised head, thorax, and abdomen/leg across various MNP loadings (detailed in Fig. 2b).

Our analysis attributes these abnormalities to the altered cardiac activity of the embryo, as revealed by the two-dimensional optical coherence tomography (2D OCT) images of the dorsal vascular system (heart) during diastole and systole of the locust embryo (see illustrative OCT images in Fig. 2c).[39,40] Specifically, the heart rate of locust embryos subjected to MNP

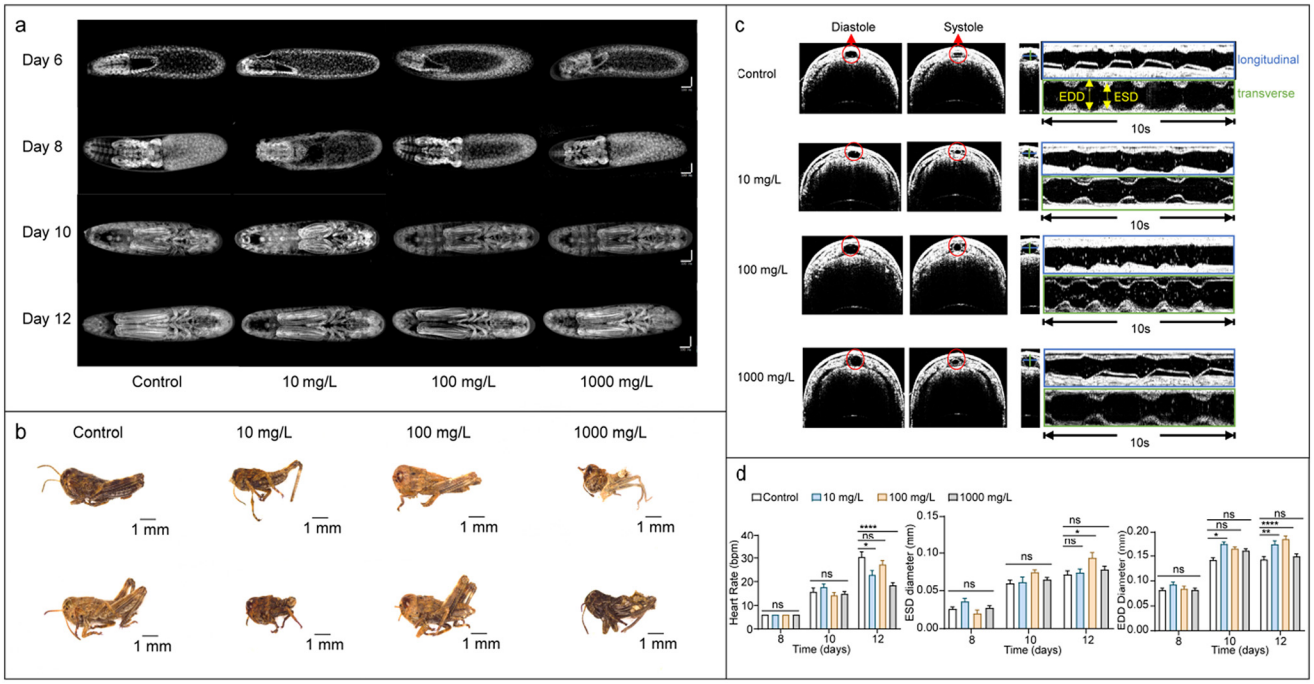

Fig. 2 The effects of different concentrations of MNPs on the development of migratory locust embryos and larvae. (a) The process of locust embryonic development over time (6–12 days). (b) The morphology of first instar larvae after hatching. (c) The end-diastolic dimension (EDD) and end-systolic dimension (ESD) images of the dorsal vascular system of locust embryos. (d) Heart rate over 10 seconds of locust embryos on days 8, 10 and 12, and EDD and ESD statistics of the embryonic dorsal vascular system. Statistical analysis was performed using multiple comparisons in three-way ANOVA tests. Bars represent the mean ± SEM (standard error of the mean), while n.s. denotes non-significant variations. *$P < 0.05$, **$P < 0.01$, ***$P < 0.001$, ****$P < 0.0001$. There are 15 locusts in each group.

treatment was significantly reduced by the 12th day of development, as compared to the control group embryos. Moreover, both the end-diastolic dimension (EDD) and end-systolic dimension (ESD) were also found to be significantly affected. Embryos treated with 100 mg L^{-1} MNPs exhibited larger ESD values, while those treated with 10 mg L^{-1} and 1000 mg L^{-1} MNPs showed slightly increased EDD values compared to the controls at the end of 12th day. It should be noted that the larger EDD values indicate diastolic filling, while increased ESD suggests weakened systolic contraction.[48] Both these abnormalities point towards compromised cardiac efficiency and are in line with the reported cardiovascular effects of nanoparticles.[49] For instance, nickel-based nanoparticles were shown to cause oxidative stress and inflammatory responses eventually leading to progression of atherosclerosis in animal models. We believe these significant changes in the ESD and EDD values suggest MNPs alter the cardiac processes through a combination of oxidative stress, nanoparticle–tissue interactions, and mechanical disruption (as observed in the μCT and SEM-EDX analyses shown in the following sections). For a summary of the heart rate, ESD and EDD variations, please see Fig. 2d.

These findings underscore the potential impact of MNPs on embryonic development and highlight the need for further investigations into their effects on cardiac function and overall morphogenesis.

Locust behavioural changes in response to nanoparticle interaction

For this experiment, jars containing egg pods were sealed and kept in a moist incubator for 10 days. After this period, the lids of the jars were removed, and jars were transferred to cages, each housing one jar, as shown in Fig. S4.† Inside each cage, Petri dishes containing water and lettuce were provided alongside each jar. Initially, the emerging nymphs were green in colour; however, due to the confinement within the cage, they turned brown in colour and started exhibiting gregarious behaviour.[5]

Following nymph emergence, 1000 mg of MNPs were sprayed onto 50 g of lettuce. Initially, the nymphs avoided the MNP-treated leaves, suggesting a repellent effect. However, as time progressed, hunger drove the nymphs to overcome their aversion and they started consuming the MNP-loaded lettuce within a few hours. The shift in the behaviour, from avoidance to consumption, was predominantly driven by the nymph's survival instincts, as they chose to eat the treated leaves rather than risk starvation. Within a day of consuming the MNP-treated lettuce, the nymphs began exhibiting signs of sluggishness and ultimately perished by the second day. This behaviour of locusts suggests that MNPs may not completely wipe out the locust populations; however, they can help in controlling and managing their numbers.

A graphical representation of the nymphs emerging and their response to MNPs is illustrated in Fig. 3(a). In jars with lower MNP loading levels, the lettuce was treated with 500 mg of MNPs (jar 2) or 100 mg of MNPs, resulting in varying stages of sluggishness and mortality in nymphs over different time frames. For instance, in the case of lettuce loaded with 500 mg of MNPs (jar 2), the nymphs remained sluggish for a few days and died between four to six days. In comparison, for the 100 mg of MNP loading on lettuce, the nymphs only became sluggish after a week, with approximately 50% dying in the subsequent week. A point to note here is that for the 100 mg MNPs batch after the initial MNP-loaded lettuce was consumed, fresh lettuce leaves were added. The trend of increasing nymph mortality enhanced by MNP loading indicates that the total amount of MNPs consumed is the determining factor. In comparison, for the control experiment, shredded lettuce without any nanoparticles had no discernible impact on the activity of the nymphs. With an adequate water supply and cage maintenance, nymphs in the control group were monitored for four weeks and all of them survived.

A deceased nymph from the cage corresponding to the 1000 mg of MNP loading was utilised for translocational studies. The μCT scan (Fig. 3b) revealed regions of varying densities, with the nymph body presenting the area of least density, primarily due to its carbon-based composition with concentrations of heavier elements, particularly in the coelomic cavity. The contrast in the μCT depends on the density and atomic number of the elements present (higher atomic numbers of Fe and Ni as compared to Si) and highlights the differences between sand grains and the MNPs based on their atomic compositions (labelled in Fig. 3b). A video showing the 3D representation of the image has been added to the ESI.†

Further confirmation of the presence of MNPs in the coelomic cavity was obtained by SEM-EDX (Fig. 3c). A cross-section of the locust stomach was utilised for the SEM-EDX, yielding peaks corresponding to the most prominent elements – Fe, Ni, O, Si, and C, with the corresponding elemental maps shown in Fig. 3d(i–v), respectively. The EDX map corresponds well with the SEM image, revealing variations in concentration intensity across different elements. The lowest brightness corresponds to carbon, representing the locust stomach, while medium brightness areas represent Si and O from the sand particles. A couple of sand particles/grains, which punctured the coelomic cavity during its cross-sectioning, can also be visualised. Brighter areas in the middle correspond to the presence of nickel ferrite MNPs, where the maps of Ni, Fe and O peaks overlap, confirming the presence of MNPs in the coelomic cavity of the locust.

In nymphs, the MNPs further interfere with the cardiac physiology. The observed reduction in heart rate and abnormalities in EDD and ESD may be linked to oxidative stress-induced mitochondrial dysfunction in cardiac cells with the uptake and translocation leading to reduced cell proliferation and metabolic activity.[46,47] Additionally, direct physical interactions between the MNPs and cardiac tissues may impair ion channel function, disrupting the electrical signalling required for rhythmic contractions.[49] Beyond ROS generation, the nanoscale size, light-dependent absorbance and chemical reactivity of MNPs may disrupt cellular signalling pathways and inhibit protein folding or DNA repair mechanisms, as observed in

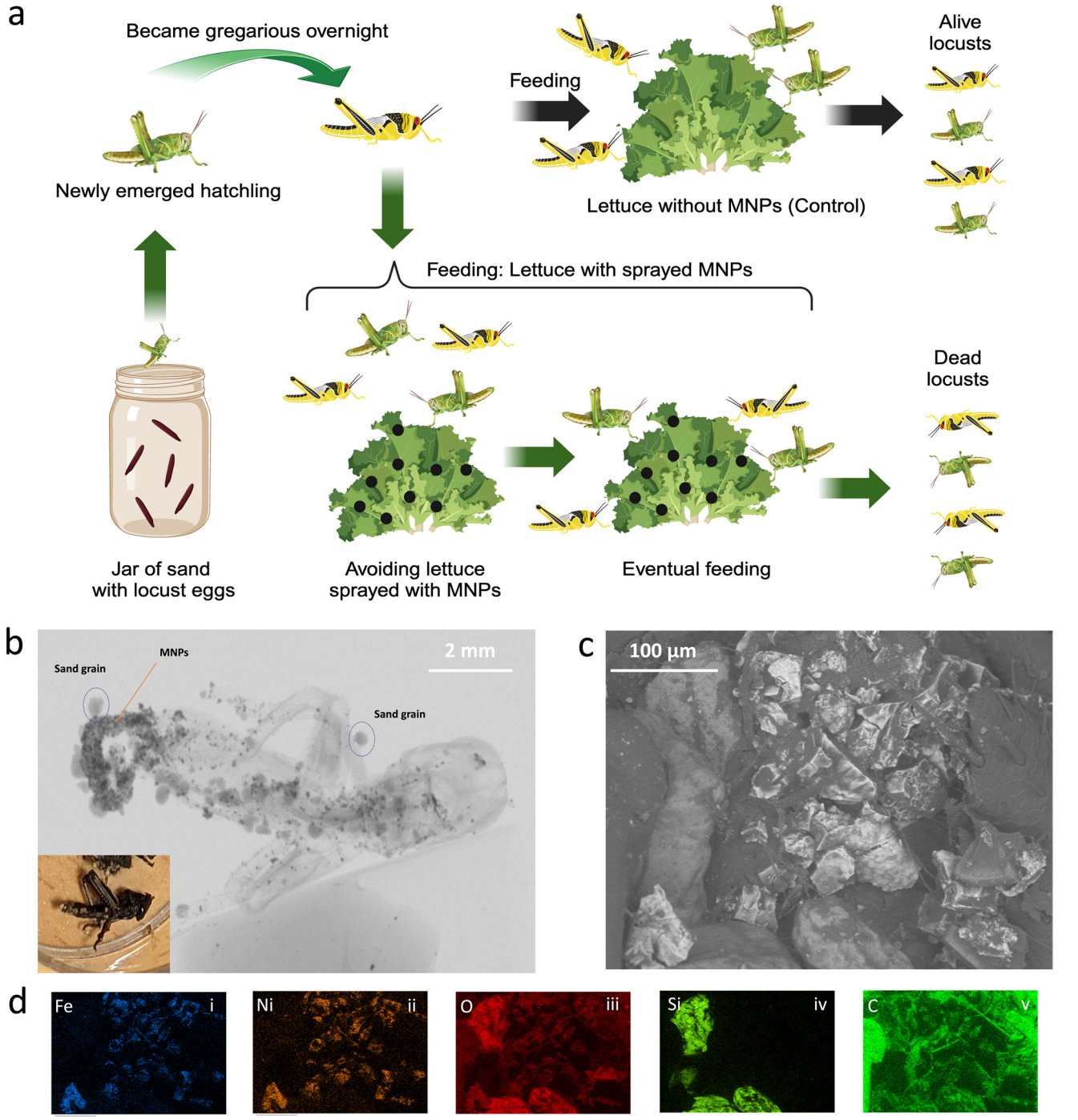

Fig. 3 Impact of MNPs on locust behaviour. (a) Scheme showing the mechanism of action of MNPs on the locust nymphs. The locusts, upon hatching from their eggs, refrain from consuming lettuce treated with MNPs initially, but eventually resort to it due to hunger, suggesting a shift in behaviour towards eating MNP-sprayed lettuce as a part of their food to survive. However, once they consume the MNP-treated lettuce, the locusts perish. Conversely, when they feed on untreated lettuce, the locusts manage to survive (control). (b) Microtomography (µCT) of nymphs after consumption of MNPs; the inset shows a photograph of a dead nymph. (c) SEM image of the stomach cross-section of the locust. (d) The elemental EDX maps corresponding to the sub-figure in (c) confirm the presence of (i) iron, (ii) nickel, (iii) oxygen, (iv) silicon, and (v) carbon, respectively.

other studies of metallic nanoparticles. Furthermore, localized mechanical stress induced by nanoparticle aggregation could impair cell division and tissue formation, exacerbating developmental delays.[50,51]

During the early growth stage, some locust nymphs did not ingest MNPs as they might have consumed parts of the lettuce devoid of MNPs. This reduced the likelihood of their exposure to MNPs at this stage. However, the probability of these locusts

eventually consuming the MNP-loaded lettuce was not eliminated. Consequently, as the nymphs matured into adults, they inevitably consumed MNPs. Our observations revealed that adult locusts that consumed MNPs survived for over two weeks. The continual presence of MNPs in their coelomic cavity suggests the potential to use these particles as markers for tracking locust movement after hatching. However, exclusive experimental studies (beyond the scope of this work) are necessary to validate the effectiveness of these MNPs as accurate tracking markers for such adult locusts.

Synergetic effects of MNPs and interplay of MNPs with sand

The synergistic effect of MNPs on the locusts was determined by loading MNPs onto newly laid eggs and subsequently exposing the emerged nymphs to the MNP-loaded lettuce.[52] Initially, 2 mL of high MNP loading (1000 mg L^{-1}) was applied to jars containing egg pods in sand. These jars were sealed to replicate prior experimental conditions and stored for 10 days, after which the seals were removed, and jars placed in a cage with water. Upon the emergence of nymphs after 14 days, they were fed with 50 g of lettuce loaded with 1000 mg of MNPs. The nymphs died within two days after consumption of MNP-loaded lettuce. The corresponding μCT of a nymph is shown in Fig. S5.†

After the nymphs had died, the jar was investigated to determine the effect of MNPs on eggs before they became nymphs. Interestingly, the egg pods located in the central portion hatched but the resulting nymphs succumbed after consuming the MNP-loaded lettuce. Conversely, egg pods located along the jar's edges failed to hatch. The μCT analysis indicated that the MNPs penetrated 7–10 cm into the sand near the jar edges but did not reach the central portions. This uneven distribution highlights the need for a deeper understanding of MNP interactions with sand to improve exposure uniformity. Fig. 4a shows a typical SEM image of sand particles, predominantly ranging from 100–200 μm, while Fig. 4b and c(i–iii) show the magnified image and the corresponding EDX spectrum/mapping, respectively.

To further investigate the distribution of MNPs in sand, μCT analysis was conducted. Due to the size constraints of the μCT instrument being unable to accommodate a 10 cm long jar (and the consequential reduction in resolution of tomograms), a smaller plastic test tube-type jar (12 mm diameter and 30 mm length) was utilised. The 2D rendered images from the μCT analysis are shown in Fig. 4d–f. For the specific experiment, 300 μL of 100 mg L^{-1} MNPs was added to the top of the jar. In the images, sand particle components were removed by digital image processing to acquire a better visualization of MNPs alone. As shown in Fig. 4g, the concentration of MNPs was observed to decrease with depth, which was attributed to the filtering effect of the sand grains. Additionally, the distribution of MNPs in the smaller jar demonstrated higher concentrations on the top (Fig. 4e, despite all efforts for a uniform distribution) and side, as compared to the centre, possibly due to differences in interaction between the solvent (suspending the MNPs) and the polystyrene container walls *versus* the sand particles. For better visualisation, a cross-sectional image is also shown in Fig. 4f. This MNP distribution pattern explains why nymphs emerged from the centre but not the sides of the jar in the synergistic experiments, highlighting the importance of understanding the interaction of MNPs with the surrounding environment for targeted interventions.

In agricultural practice, where large areas are treated as opposed to small-scale jar experiments, uniform lateral distribution of MNPs is crucial. In our experiments, μCT images (Fig. 4g) were utilised for the determination of the MNP density along the depth. As the container had a semi-spherical bottom, the depth of uniform diameter, corresponding to 28 mm, was utilised to determine the density, which was subsequently converted to changes in the concentration of MNPs based on a quadratic fit (further details are given in the ESI† section).

The derived fitting parameters were then utilised to determine the concentration of the MNPs at various depths. Depths of up to 100 mm were used for determining the concentration change for various starting concentrations. As shown in the figure, at lower concentrations, the MNPs were unable to reach deeper depths, while at higher concentrations (1000 mg L^{-1}), MNPs were observed up to 10 cm in depth. This indicates that the depth of MNPs inside the soil can be controlled and adjusted by varying the concentration of the MNPs. Future experimental studies could explore the transfer of MNPs through sand, examining factors such as MNP aggregation in water, or their transfer characteristics through sand particles.[53] Understanding these dynamics could provide valuable insights for optimising the application of MNPs in agriculture and enhancing their efficacy in targeted pest control strategies.

Plasmonic contributions of $NiFe_2O_4$ nanoparticles to the disruption of locust embryo development

The plasmonic characteristics of $NiFe_2O_4$ arising from localized surface plasmon resonances (LSPRs) are relevant to understanding their effects on locust embryos. LSPRs occur when conduction electrons in the nanoparticles collectively oscillate upon exposure to electromagnetic radiation, particularly in the visible and near-infrared (UV-vis) regions. Multiple previous studies provide direct evidence of LSPRs in $NiFe_2O_4$ nanoparticles as they absorb light in the UV-vis region.[54–57] The plasmonic property is primarily due to the presence of the nickel element.[58,59] The Raman spectrum shown in Fig. S1b† of this study reveals the characteristic vibrational modes of spinel ferrites. While primarily used for structural confirmation, the Raman signal intensity may be enhanced by LSPR effects, supporting nanoparticle interactions with biological systems. The plasmonic features of nanoparticles contribute to the observed developmental abnormalities in locust embryos through multiple mechanisms. LSPR excitation generates hot electrons and enhances local electric fields, promoting ROS formation,[60] which induces oxidative stress, disrupting cell signalling, protein stability, and membrane integrity, ultimately leading to developmental delays and cardiac dysfunction. Additionally, the plasmonic properties enable localized photo-

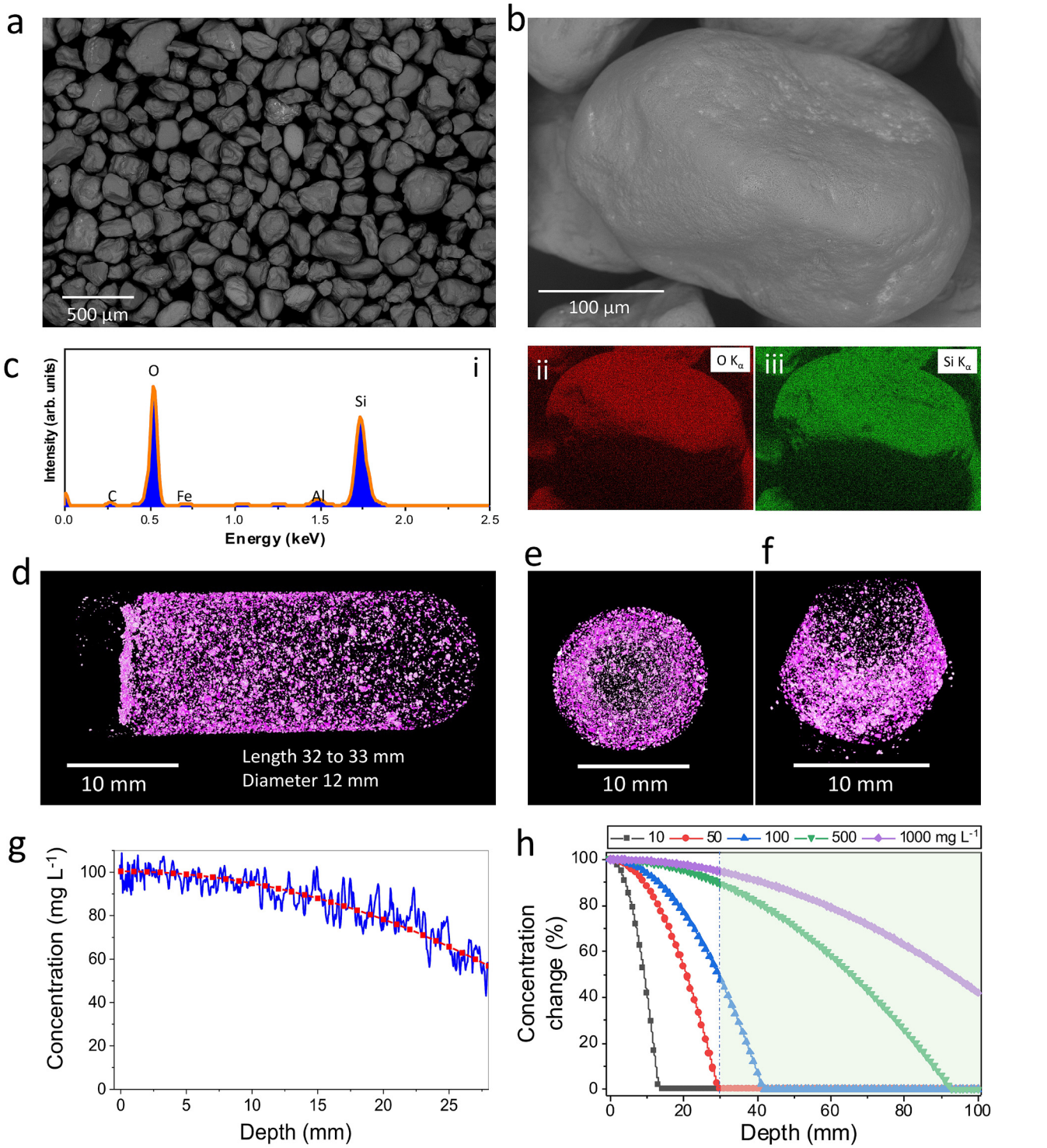

Fig. 4 Study of synergistic effects. (a) Low and (b) high magnification SEM images of grains of sand (local environment of locust eggs) within which locust eggs thrive. (c) The EDX spectrum and the O and Si elemental maps from a grain of sand (shown in (b)). (d) μCT showing the distribution of MNPs in the sand (digitally removed) viewed from the side, (e) from the top and (f) along the cross-section of the jar. (g) The μCT intensity was utilised for the determination of the concentration of MNPs at various depths. (h) Concentrations of MNPs at various depths for solutions with different concentrations of MNPs.

thermal heating upon light exposure,[61] which, although not directly quantified in this study, is well documented in the literature and likely contributes to blastokinesis disruption and cellular destabilisation in locust embryos. Furthermore, the plasmonic behaviour enhances interactions with electromagnetic fields, influencing nanoparticle mobility in soil and

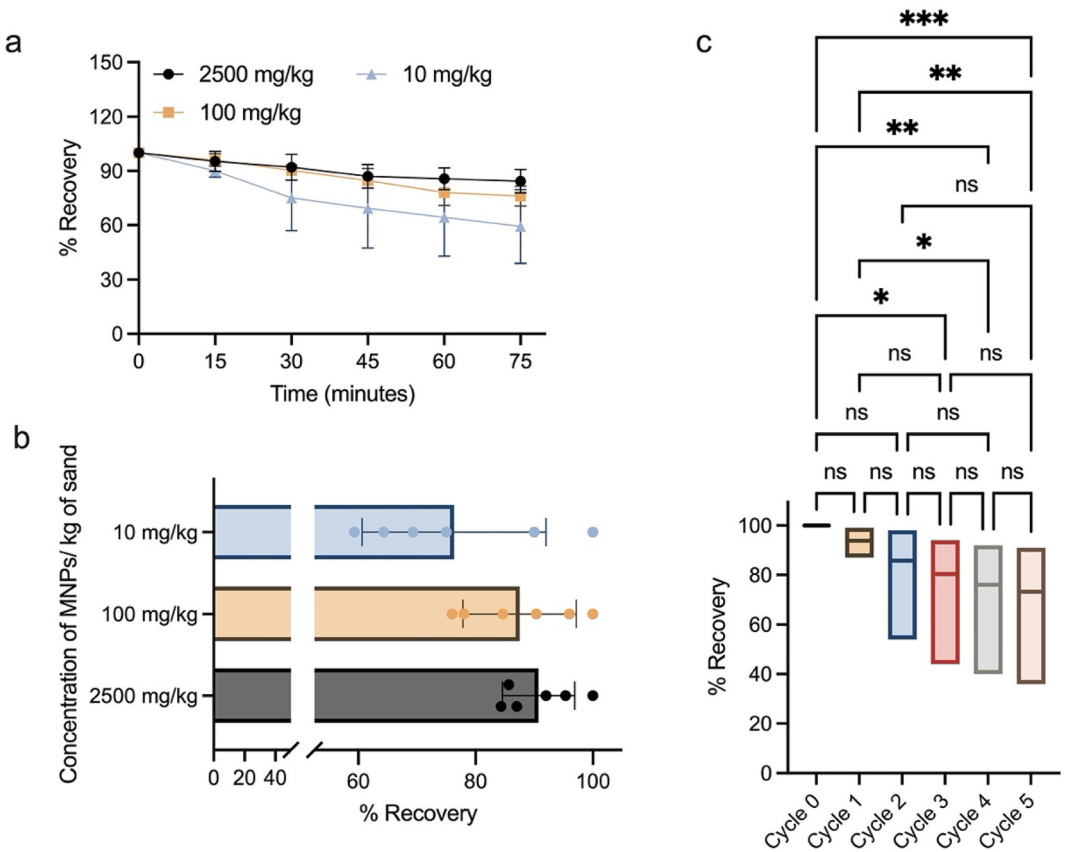

Fig. 5 The fate of nanoparticles in soil. (a) Recovery of MNPs (%) from sand for various initial concentrations of MNPs over 75 minutes. (b) Recovery of MNPs (%) from sand for various initial concentrations of MNPs after 5 cycles. (c) Statistical significance between different recovery cycles is represented by the p values where $p > 0.05$ is not significant (ns). $p < 0.05$, $p < 0.01$ and $p < 0.001$ are represented by (*), (**) and (***), respectively.

penetration into locust eggs, facilitating translocation and targeted deposition in embryonic regions, as confirmed by μCT and SEM-EDX analyses.

Recovery of unused MNPs from soil

To evaluate the reusability and extraction of MNPs, experiments were conducted to recover MNPs from sand using magnetic collection. This method has proven to be rapid, convenient, and efficient for the recovery of magnetic nanoparticles.[62] For this investigation, different initial concentrations of MNPs (in powdered form), ranging from 10 to 2500 mg MNPs per kg of sand, were mixed thoroughly with sand. Thereafter, a 5 mm neodymium magnet (from RS Scientific, UK) was used for the recovery of MNPs. Once retrieved, the MNPs were reintroduced into fresh sand to evaluate the recovery process and this cycle was repeated. The change in recovery concentration over time is shown in Fig. 5 and Table S1.† Remarkably, even after 5 recovery cycles, approximately 90% of MNPs (for an initial concentration of 2500 mg MNPs per kg of sand) and approximately 70% of MNPs from other lower concentrations of MNPs in sand were recovered. This underscores the promising potential for the reusability of these MNPs from sand/soil. The low recovery rate for the 10 mg kg^{-1} sample may be attributed to factors such as measurement errors in weighing, potentially undiscovered areas in the sand that have MNPs, and the strong binding of MNPs to the recovery magnet, particularly impacting lower concentrations more significantly than the higher concentrations. Practically, magnetic plough blades or magnets attached to plough blades can be used for efficient and effective recovery. The MNPs, once recovered, can be reused for several cycles reducing the economic and environmental strain, highlighting a sustainable approach for nanoparticle utilisation in agriculture.

Conclusions

This study highlights the promising potential of nickel ferrite magnetic nanoparticles (MNPs) as an effective tool for combating locust infestations. By initially loading the locust eggs with MNPs, a significant reduction in the locust population can be achieved, with a high likelihood of most nymphs being eradicated owing to delayed embryonic growth and disruption of the blastokinesis process. In cases where some egg pods evade exposure to the MNPs, newly hatched locusts are deterred from feeding on MNP-treated plants and ultimately perish if

they attempt to consume them. Given the capacity of locust swarms to travel vast distances and consume massive quantities of crops daily, their impact on food security is profound. Our findings demonstrate how innovative nanotechnologies can be leveraged to address these challenges. Looking ahead, integrating MNPs with entomopathogenic fungi offers the potential to further enhance the effectiveness of locust management strategies. This combined approach could significantly contribute to global efforts to achieve sustainable development goals by 2030.

Materials and methods

Materials

Nickel chloride hexahydrate, iron(III) chloride hexahydrate and sodium hydroxide were obtained from Sigma Aldrich and used without any further purification. Deionised water (18 MΩ·cm) was obtained from ELGA Purelab deionised water equipment. Locust eggs were obtained from Darwin Biological, UK.

Nanoparticle synthesis

$NiFe_2O_4$ was prepared using a co-precipitation method wherein stoichiometric proportions of high purity nickel chloride hexahydrate and iron(III) chloride hexahydrate were dissolved in boiling 0.40 M NaOH under vigorous stirring.[25] After cooling to room temperature, the resulting precipitate was washed with distilled water until a neutral pH (7) was achieved, and then centrifuged to collect the residue. The residue was dried overnight in an oven at 50 °C and subsequently calcinated at 800 °C for 3 h in a muffle furnace, with heating and cooling rates of 200 °C h^{-1}.

Material characterisation

Nanomaterials were characterised using a variety of techniques. Scanning electron microscopy-energy dispersive X-ray analysis (SEM-EDX) was performed on a Hitachi SU5000 field emission microscope coupled with an Oxford Instruments 80 mm^2 X-Max EDX detector in low vacuum mode using a back-scattered electron detector at 10 kV. Transmission electron microscopy measurements were performed at 200 kV using a Jeol JEM-2100F system. Raman spectroscopy measurements were performed on a Renishaw inVia Qontor® spectrometer using a 785 nm laser at 1% laser power with exposure time of 10 s. Powder X-ray diffraction measurements were performed in the locked-couple mode over a 10–80° range using a Panalytical Empyrean Series 3 system.[25]

Growing locusts in Petri dishes

The eggs were received in jars filled with sand from Darwin Biological (UK). The locust eggs were collected using the following protocol. Silver sand was prepared by washing sand repeatedly under tap water followed by drying in a saucepan with occasional stirring. Once dried and cooled, 15 wt% water was added to the sand and mixed thoroughly. The moist sand was then transferred to a cylindrical jar (10 cm length and 5 cm diameter). It was ensured that sand had no air-gaps and was not compacted. The jars were kept in locust cages allowing locusts to lay eggs in the sand. For every batch, two jars containing 2 or 3 egg pods (mostly two, except for one jar from batch 3) were received (Fig. 1). The pods were buried approximately 7–10 cm deep and contained around 50–70 eggs. The eggs were ellipsoidal, measuring 5–7 mm in length and 1–2 mm in diameter. A germinal disk was visible on the bottom of each egg.

Growth of locust eggs and effect of nanoparticles

To assess the impact of MNPs on eggs, three concentrations of 10 mg L^{-1}, 100 mg L^{-1}, and 1000 mg L^{-1}, referred to as low, medium, and high loadings, were tested alongside a control group. Experiments were conducted using 12-well plates, typically used for cell cultures. Four eggs were placed in each well, totalling 48 eggs (12 × 4) per experimental condition. Eggs were buried in sand, and 300 μL of tap water (control) or tap water containing MNPs was added to each well to maintain adequate humidity for growth. The well plates were then placed in an incubator at 30 °C with 90% humidity.

For the growth study, 3 eggs were placed in each of the 21 wells, with each well corresponding to a specific day of growth (using two 12-well plates). Each day, the eggs from one of the wells were removed for at different growth stages.

Exposure of nanoparticles to nymphs and adult locusts

For determining the effect of nanoparticles on the locusts, jars containing egg pods were sealed and kept in a moist incubator for 10 days. After this period, the lids of the jars were removed, and jars were transferred to cages, each housing one jar, as shown in Fig. S4.† Inside each cage, Petri dishes containing water and lettuce were provided alongside each jar. Following nymph emergence, 1000 mg of MNPs was sprayed onto 50 g of lettuce and its effect was observed by regular monitoring of the cage.

To assess the effect on adult locusts, five adult locusts were placed in a cage with 1000 mg MNP-loaded lettuce (50 g).

In another experiment, MNPs were loaded onto the eggs, and the emerging nymphs were exposed to the MNP-loaded lettuce as well. The loading was similar to the individual tests.

Nanoparticle recovery experiments

To determine the reusability of the MNPs, various amounts of MNPs were mixed with sand followed by recovery cycles. Specifically, samples of 10, 100 and 2500 mg MNPs per kg of sand were prepared. The MNP-in-sand mixtures were subjected to several cycles of the recovery process to determine the reusability of the MNPs at different loadings. The experiments were run in triplicate to obtain statistically significant data.

Micro-CT analysis of locusts

X-ray micrographs (micro-computed tomography, μCT) were obtained on a Bruker X-ray Microtomograph SkyScan 1275 with a source voltage of 40 kV and source current of 220 μA. The μCT resolution depends on the distance of the object from

the X-ray source. For these samples, due to the finite size of eggs and hatchlings, the pixel size (resolution) was around 10 μm.

Data availability

All experimental data are shared in this work and any other related data are available on request to the corresponding author.

Conflicts of interest

There are no conflicts to declare.

Acknowledgements

The authors would like to thank the Department of Economy, Northern Ireland's Global Challenges Pump Primer Fund for supporting this project. The study was also supported by the project of the High-level Talent Team Construction in Hebei (No. 225A4203D). Artwork featured in TOC is created in BioRender. Bhalla, N. (2025) **https://BioRender.com/t03z377** and the artwork featured in Figure 3 is also created in BioRender. Bhalla, N. (2025) **https://BioRender.com/b24i239**.

References

1 S. J. Simpson and G. A. Sword, *Curr. Biol.*, 2008, **18**.
2 U. Riaz and K. R. Hakeem, *Locust Outbreaks: Management and the World Economy*, 2023, vol. 1.
3 N. P. Singh and V. Kumari, *Locusts. Polyphagous Pests of Crops*, 2021, vol. 1.
4 X. Wang, X. Fang, P. Yang, X. Jiang, F. Jiang, D. Zhao, B. Li, F. Cui, J. Wei, C. Ma, Y. Wang, J. He, Y. Luo, Z. Wang, X. Guo, W. Guo, X. Wang, Y. Zhang, M. Yang, S. Hao, B. Chen, Z. Ma, D. Yu, Z. Xiong, Y. Zhu, D. Fan, L. Han, B. Wang, Y. Chen, J. Wang, L. Yang, W. Zhao, Y. Feng, G. Chen, J. Lian, Q. Li, Z. Huang, X. Yao, N. Lv, G. Zhang, Y. Li, J. Wang, J. Wang, B. Zhu and L. Kang, *Nat. Commun.*, 2014, **5**, 2957.
5 C. M. Topaz, M. R. Orsogna, L. Edelstein-Keshet and A. J. Bernoff, Locust Dynamics: Behavioral Phase Change and Swarming, 2012, **8**, 1002642.
6 P. M. Symmons, K. Cressman and L. O. Fresco, *Desert Locust Guidelines 1. Biology and behaviour*, 2001.
7 S. C. Ma, *Acta Entomol. Sin.*, 1958, **8**, 1–40.
8 X. Wang and L. Kang, *Annu. Rev. Entomol.*, 2014, **59**, 225–244.
9 2024, **https://www.fao.org/locusts/en/** (accessedApril14).
10 J. Qiu, *Nature*, 2009, DOI: **10.1038/news.2009.978**.
11 Q. Tang, J. Feng, D. Zong, J. Zhou, X. Hu, B. Wang and T. Wang, *Diversity*, 2023, **15**, 1038.
12 J. P. Youngblood, A. J. Cease, S. Talal, F. Copa, H. E. Medina, J. E. Rojas, E. V. Trumper, M. J. Angilletta and J. F. Harrison, *Ecol. Monogr.*, 2023, **93**, 1550.
13 B. Huang, F. Chen, Y. Shen, K. Qian, Y. Wang, C. Sun, X. Zhao, B. Cui, F. Gao, Z. Zeng and H. Cui, Advances in Targeted Pesticides with Environmentally Responsive Controlled Release by Nanotechnology, *Nanomaterials*, 2018, **8**, 102.
14 X. Mao and Z. Yang, *J. Nanopart. Res.*, 2023, **25**, 1.
15 S. P. Dalmolin, D. B. Dreon, F. V. Thiesen and E. Dallegrave, *Environ. Toxicol. Pharmacol.*, 2020, **75**, 103304.
16 **https://www.chefsbest.com/advantages-disadvantages-pesticides/**.
17 J. A. Siddiqui, R. Fan, H. Naz, B. S. Bamisile, M. Hafeez, M. I. Ghani, Y. Wei, Y. Xu and X. Chen, *Front. Physiol.*, 2023, **13**, 1112278.
18 S. Vaidya, C. Deng, Y. Wang, N. Zuverza-Mena, C. Dimkpa and J. C. White, *NanoImpact*, 2024, **34**, 100502.
19 R. Urkude, Application of Nanotechnology in Insect Pest Management, *Int. Res. J. Sci. Eng.*, 2019, **7**, 151.
20 R. Periakaruppan, V. Romanovski, S. K. Thirumalaisamy, V. Palanimuthu, M. P. Sampath, A. Anilkumar, D. K. Sivaraj, N. A. N. Ahamed, S. Murugesan, D. Chandrasekar and K. S. V. Selvaraj, *ChemEngineering*, 2023, **2023**, 61.
21 H. Liu, W. Shangguan, P. Zhao, C. Cao, M. Yu, Q. Huang and L. Cao, *Size Effects of Nanoenabled Agrochemicals in Sustainable Crop Production: Advances, Challenges, and Perspectives*, 2024.
22 D. Wang, N. B. Saleh, A. Byro, R. Zepp, E. Sahle-Demessie, T. P. Luxton, K. T. Ho, R. M. Burgess, M. Flury, J. C. White and C. Su, *Nat. Nanotechnol.*, 2022, **17**, 347–360.
23 M. Vishnu, M. Kannan, R. P. Soundararajan, A. Suganthi, A. Subramanian, M. Senthilkumar, K. Rameash, K. Madesh and K. Govindaraju, *Nano-bioformulations: emerging trends and potential applications in next generation crop protection*, 2024.
24 D. Martínez-Cisterna, O. Rubilar, G. Tortella, L. Chen, M. Chacón-Fuentes, M. Lizama, P. Parra and L. Bardehle, *Molecules*, 2024, **29**, 5520.
25 P. Sharma, A. Sharma, M. Sharma, N. Bhalla, P. Estrela, A. Jain, P. Thakur and A. Thakur, *Global Challenges*, 2017, **1**, 1700041.
26 F. M. Hashem, E. Elgazzar and W. A. Mostafa, *BMC Chem.*, 2023, **17**, 7.
27 M. Colombo, S. Carregal-Romero, M. F. Casula, L. Gutiérrez, M. P. Morales, I. B. Böhm, J. T. Heverhagen, D. Prosperi and W. J. Parak, *Chem. Soc. Rev.*, 2012, **41**, 4306–4334.
28 R. Pazik, A. Ziecina, E. Zachanowicz, M. Małecka, B. Poźniak, J. Miller, Z. Śniadecki, N. Pierunek, B. Idzikowski, L. Mrówczyńska, A. Ekner-Grzyb and R. J. Wiglusz, *Eur. J. Inorg. Chem.*, 2015, **2015**, 4750–4760.

29 C. Guo, R. J. Weber, A. Buckley, J. Mazzolini, S. Robertson, J. M. Delgado-Saborit, J. Z. Rappoport, J. Warren, A. Hodgson, P. Sanderson, J. K. Chipman, M. R. Viant and R. Smith, *Int. J. Mol. Sci.*, 2021, **22**, 1–24.
30 T. H. Shin, C. Seo, D. Y. Lee, M. Ji, B. Manavalan, S. Basith, S. K. Chakkarapani, S. H. Kang, G. Lee, M. J. Paik and C. B. Park, *Arch. Toxicol.*, 2019, **93**, 1201–1212.
31 M. Awashra and P. Młynarz, *The toxicity of nanoparticles and their interaction with cells: an in vitro metabolomic perspective*, 2023.
32 M. S. Khan, S. A. Buzdar, R. Hussain, G. Afzal, G. Jabeen, M. A. Javid, R. Iqbal, Z. Iqbal, K. B. Mudassir, S. Saeed, A. Rauf and H. I. Ahmad, *Oxid. Med. Cell. Longevity*, 2022, **2022**, 5066167.
33 F. Ahmad, X. Liu, Y. Zhou and H. Yao, *Aquat. Toxicol.*, 2015, **166**, 21–28.
34 P. K. Sharma, P. Sharma, S. Biswas and A. K. Nagawat, *AIP Conf. Proc.*, 2013, **85**, 85–86.
35 A. Pathania, K. Rana, N. Bhalla, P. Thakur, P. Estrela, J. L. Mattei, P. Queffelec and A. Thakur, *J. Mater. Sci.: Mater. Electron.*, 2017, **28**, 679.
36 K. Nejati and R. Zabihi, *Chem. Cent. J.*, 2012, **6**, 1.
37 C. Sedrati, S. Alleg, H. Boussafel and A. B. Hacine, *J. Mater. Sci.: Mater. Electron.*, 2021, **32**, 24548.
38 S. Modak, M. Ammar, F. Mazaleyrat, S. Das and P. K. Chakrabarti, *J. Alloys Compd.*, 2009, **473**, 15–19.
39 Y. Su, J. Fan, X. Wang, X. Wang, J. Li, B. Duan, L. Kang, L. Wei and X. S. Yao, *J. Biophotonics*, 2022, **15**, e202100308.
40 Y. Su, L. Wei, H. Tan, J. Li, W. Li, L. Fu, T. Wang, L. Kang and X. S. Yao, *J. Biophotonics*, 2020, **13**, e201960047.
41 K. O. Maeno, C. Piou and N. Leménager, *J. Insect Physiol.*, 2023, **145**, 104467.
42 S. Donoughe, *Curr. Opin. Insect Sci.*, 2022, **50**, 100868.
43 Y. Nishide, S. Tanaka and S. Saeki, *J. Insect Physiol.*, 2015, **76**, 24.
44 D. Tari, S. Haryan, K. Patankar, V. Jaiswal, M. Samant, S. Sivakami and P. M. Dongre, *Curr. Sci.*, 2017, **112**(7), 1574–1578.
45 M. Awashra and P. Młynarz, *The toxicity of nanoparticles and their interaction with cells: an in vitro metabolomic perspective*, 2023.
46 M. T. Zhu, B. Wang, Y. Wang, L. Yuan, H. J. Wang, M. Wang, H. Ouyang, Z. F. Chai, W. Y. Feng and Y. L. Zhao, *Toxicol. Lett.*, 2011, **203**, 162–171.
47 G. S. Kang, P. A. Gillespie, A. Gunnison, A. L. Moreira, K. M. Tchou-Wong and L. C. Chen, *Environ. Health Perspect.*, 2011, **119**, 176–181.
48 E. A. Salzen, *Development*, 1960, **8**, 139–162.
49 C. Huang, X. Liu, Q. Wu, J. Cao, X. Zhu, X. Wang and Y. Song, *Cardiovascular toxic effects of nanoparticles and corresponding molecular mechanisms*, 2024.
50 X. Zhao, H. Xu, Y. Li, Y. Liu, X. Li, W. Zhou, J. Wang, C. Guo, Z. Sun and Y. Li, *Sci. Total Environ.*, 2022, **842**, 156854.
51 S. A. Oakes and F. R. Papa, *Annu. Rev. Pathol.: Mech. Dis.*, 2015, **10**, 173–194.
52 S. Li, S. Feng, H. Ullah, X. B. Tu and Z. H. Zhang, *J. Integr. Agric.*, 2022, **21**, 3467.
53 P. L. Chariou, A. B. Dogan, A. G. Welsh, G. M. Saidel, H. Baskaran and N. F. Steinmetz, *Nat. Nanotechnol.*, 2019, **14**, 712.
54 S. Khamari, A. Kumar, N. Mohapatra and R. Jha, *IEEE Sens. J.*, 2022, **22**, 4014–4021.
55 R. Hariharasuthan, S. Chitradevi, K. S. Radha and V. Chithambaram, *Appl. Phys. A*, 2022, **128**, 1045.
56 L. Mahmudin, Y. Ndora and M. S. Ullum, 4th International Seminar on Science and Technology (ISST 2022), 2023, pp. 109–113.
57 M. B. Taj, M. D. Alkahtani, A. Raheel, S. Shabbir, R. Fatima, S. Aroob, R. Yahya, W. Alelwani, N. Alahmadi and M. Abualnaja, *Sci. Rep.*, 2021, **11**, 5439.
58 J. Chen, P. Albella, Z. Pirzadeh, P. Alonso-González, F. Huth, S. Bonetti, V. Bonanni, J. Åkerman, J. Nogués and P. Vavassori, *Small*, 2011, **7**, 2341–2347.
59 V. Bonanni, S. Bonetti, T. Pakizeh, Z. Pirzadeh, J. Chen, J. Nogués, P. Vavassori, R. Hillenbrand, J. Åkerman and A. Dmitriev, *Nano Lett.*, 2011, **11**, 5333–5338.
60 R. Canaparo, F. Foglietta, T. Limongi and L. Serpe, *Materials*, 2020, **14**, 53.
61 W. He, X. Huang, X. Ma and J. Zhang, *J. Opt.*, 2022, **51**, 142–153.
62 M. Miceli, P. Frontera, A. Macario and A. Malara, *Catalysts*, 2021, **11**, 591.